Computed Tomography Image based Classification and Detection of Lung Diseases with Image Processing Approach

R.Deenadhayalan[1], Dr.N.Krishnamoorthy[2], Dr. Madasamy Raja. G[3] , Galiveeti Poornima[4], Dr. Sabera Begum[5] , Dr. C M Velu[6]

[1]Assistant Professor, Department of Information Technology, Paavai Engineering College, Namakkal, Tamilnadu , India.

[2]Associate Professor, Department of Computer Science and Engineering, Kongu Engineering College, Perundurai, India.

[3]Associate Professor, Department of Information Technology, Paavai Engineering College, Namakkal, Tamilnadu , India.

[4]Assistant Professor, Department of Computer Science and Engineering, Presidency University, Bangalore, Karnataka, India.

[5]Professor & HoD, Department of Computer Science and Engineering, K.C.T.Engineering College, Kalaburagi, Karnataka, India.

[6]Professor, Department of Computer Science and Engineering, Saveetha School of Engineering, Saveetha University, SIMATS, Chennai, Tamilnadu , India.

Abstract

Oncology relies heavily on the process of tumour detection. The broad computer vision issues of image augmentation, segmentation, and classification are of primary significance in medical imaging. Due to its excellent spatial resolution, quick imaging speed, and widespread availability, computed tomography (CT) is one of the most often utilised imaging modalities for tumour detection and diagnosis in particular. Additionally, the most used imaging method for diagnosing lung tumours is computed tomography (CT). With computed tomography, nodules and diseased remnants of various diameters may be easily seen. There are two types of lung nodules: benign and malignant. Solid and unusual nodules may sometimes be diagnosed as malignant during the diagnostic process. However, a solid lump with calcification is often classified as benign in most circumstances. To expedite therapy, it is critical to detect nodules as soon as possible. As a result, computed tomography's complex and hard duties for lung tumour identification and classification in medical image processing. Additionally, an image enhancement method could increase the precision of the procedures for identifying and classifying tumours. The main goal of this study is to provide an effective system for an automated diagnosis of lung tumours.

Keywords: Computed Tomography Image, Segmentation, Tomography, Tomography Images and Tumour Detection

Number: 10.14704/nq.2022.20.9.NQ44321 **Neuro Quantology 2022; 20(9):2743-2756**

1. Introduction

These days, cancer is a deadly illness. Figure.1. is a graph showing the tumour response rates to polymer-drug conjugates (PDCs). Numerous types of tests, including Computed Tomography (CT), Positron Emission Tomography (PET), and Magnetic Resonance Imaging (MRI), are necessary to identify and treat this malignant condition as soon as feasible. Every imaging modality has a unique imaging process to provide a variety of valuable information. Among these, computed tomography (CT) is the most reliable and accurate. Oncologists, radiologists, and other medical professionals spend a lot of effort segmenting medical pictures for successful treatment planning in actual

medical diagnosis. The entire 3D bio-structure is not taken into consideration when labelling brain tumours in CT scans, and this results in substantial disagreement across specialists [1]. The use of computer-aided tumour segmentation systems in medical image analysis is crucial. The creation of a system for analysing medical images not only reduces physicians' mistake and burden, but it also allows for the quantification of changes in lung tumours during the course of therapy. However, there are still a lot of different types of tumours with morphological variability, a variety of shapes, appearance properties among individuals, and the deformation near the structures, which results in an abnormal geometry for healthy tissues and lack of knowledge about them, making it a challenging problem to automatically segment tumour regions from CT multi-sequences.

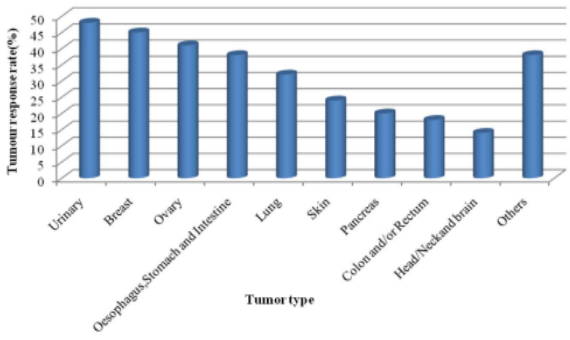

Figure.1. Graphical representation of the tumour response rates for polymer-drug conjugates (PDCs)

In order to concentrate on semi-automatic or fully-automatic segmentation techniques on repeated CT scans for medical research, illness monitoring, therapeutic control, and other purposes, it is practicable. Different CT sequences from varied excitations may reflect pathological information about the tumours and give different and somewhat independent information about various organs. The CT alone cannot provide comprehensive information on aberrant tissues since the tumour is made up of several biological tissues. Bringing together many complementing pieces of information helps improve tumour segmentation. To determine the location, extent, prognosis, and diagnosis of the tumours, radiology specialists always aggregate the multi-spectral CT data of a single patient. The radiological modality of computed tomography (CT) provides clinical information for the identification, categorization, and delineation of the illness. It is widely recognised as an addition to supplemental imaging techniques and is the first diagnostic modality for a variety of issues. Medical CT pictures are an extremely significant application area in this theory. Therefore, it is crucial that a proper introduction to CT be provided.

In conventional X-ray imaging, the body's entire thickness is projected onto a film; structures superimpose and are exceedingly challenging to distinguish. The lack of knowledge regarding its depth is one of the issues. Let's say a front-to-back chest shot shows a little lung cancer (Figure.2. (a)). The radiologist lacks the expertise to determine the exact location of this cancer both forward and backward. But even when the cancer may go behind the rib, it is still feasible to take a lateral shot (a side view). A cross-sectional picture is essential in these circumstances Figure 2. (b). When Geoffrey N. Hounsfield presented the first CT scanner in 1972, this really became a reality. Computed tomography (CT), a cutting-edge imaging technique, reconstructs a cross-sectional picture of the body from a "virtual pile of X-ray photos." The representation of a slice across the body in a tomographic picture. Tomography is a word with Greek roots. Greek words like "tomos" and "graphein" signify to cut and write, respectively. As a result, "writing slices" are precisely what the term "tomography" alludes to. Structures and lesions that were previously impossible to see are now visible with a great deal of clarity. Figure 3 provides the CT scanner's schematic design. A thin, collimated X-ray beam passes through the body as a detector to gauge the intensity being conveyed. The collimator produces a narrow, straight X-ray beam by using a collection of thin lead tubes or a grid of tiny holes in a lead plate. As the source and detector are carried past the body together, measurements are made at a great number of different locations. The apparatus is then slightly turned around the body axis and examined once again. This is repeated 180 times at 1° intervals. Several points of each scan's intensity of the transmitted beam are sent to a computer, which reconfigures the slice's picture at each angle and for each intensity level. The image is reflected on a computer monitor.

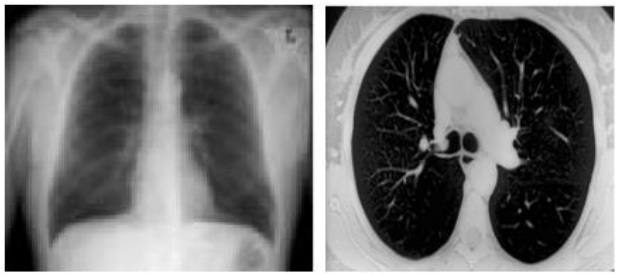

Figure.2. (a) Typical AP (anterior-posterior or front-to-back) chest X-ray photograph, (b) Transversal CT slice of the chest

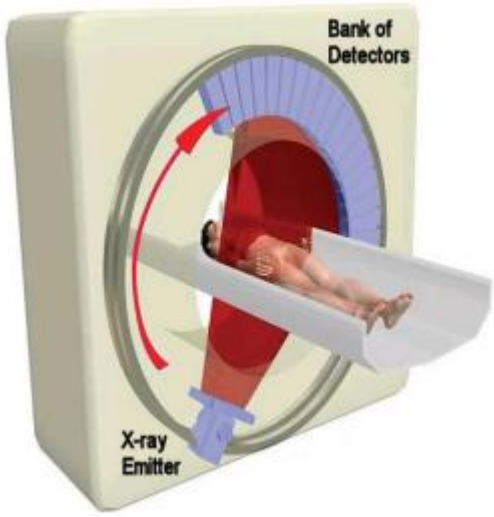

Figure.3. Schematic diagram of CT scanner

2. Literature Survey

This study was motivated by a number of prior studies on medical image processing that deal with picture enhancement and tumour identification on medical images. We study a number of cutting-edge methods for medical picture applications. The approaches for medical image enhancement, segmentation, and classification that have been created to date against medical images like computed tomography (CT), positron emission tomography (PET), and magnetic resonance imaging have been surveyed and categorised in this area (MRI).

According to Grau et al., fast and suitable segmentation algorithms play a critical role in the diagnosis, classification, and quantitative description of illnesses in diverse tissues, including liver tumours (2004). For automated liver perfusion analysis, which provides useful information on the blood flow to the liver as in [4], accurate segmentation of the liver using MRI images is necessary, for instance, in clinical surgery. Given that the gray-level distribution of the surrounding organs is little distinct, precise liver segmentation in abdominal MRIs is a difficult undertaking. Since the border regions between the liver and the surrounding tissues often have uniform intensity distributions, this usually makes the liver more segmented than it should be. Additionally, the segmentation leakage as shown in [5] is often caused by the vasculature inside the liver. The primary cause of the abdominal MRI research's limitations is that artefacts have a significant negative impact on these pictures. Additionally, as demonstrated in [6], they have a poor gradient response, which makes accurate liver segmentation very challenging. To classify tumour tissues at the pixel level, a variety of strategies that have not been verified by [7] or implemented by [8] categorization have been introduced. It is very difficult to continue in an unsupported manner while segmenting brain tumours since there are no priors on the tumours' morphology or severity. Prior information is taken into account by model-based approaches, such as shape and texture data involving a collection of pixels. For a variety of tumours and tissues, [9] introduces a probabilistic geometric model incorporating picture registration and spatial prior information. For monitoring tumours in the heart and brain, [10] uses a hybrid deformable model coupled with shape, texture, graphical representations, and a learning step. In [11], a two-step segmentation approach is used in the practical diagnosis of different types of tumours. The initial findings are first refined by the combination of stringent spatial restrictions and a deformable model. The registration-based segmentation techniques that are also widely utilised for brain segmentation and the follow-up system include atlas-based elastic transformation by [12] and follow-up approach in [13]. The algorithm put forth in [14] is known as registration optimization of tumour parameters and registration of brain images with tumours (ORBIT), and it consists of three parts: a replication model for tumour growth and mass effect, a deformable registration technique for images bearing tumours, and an optimization approach for evaluating the constraints of the tumour growth and mass effect model. It is suitable for tumours with clear boundaries, but it is limited by previous tissue

segmentation, especially in the vicinity of the tumours, where edoema and infiltration often manifest. Initiated in [15], an improved mountain clustering technique uses the cluster entropy as a metric for quantitative comparison of various cluster algorithms. Setting aside portions of the data set based on step-by-step clustering is the key idea behind this approach to reduce processing complexity. It produces greater accuracy when compared to k-means and FCM. Ingeniously developed by [16], Fluid Vector Flow (FVF) is another active-contour model that tracks the contours of brain tumours in 2D MRI images by capturing a wide variety of concave forms. The method is tested on artificial pictures, head MRI scans, and brain tumour MRI scans. Even though tracking brain tumours takes a long time, it still performs amazingly. By using closest neighbour pattern matching, the method described in [17] generates a probability map of disease, which is then segmented in place of the input intensity picture. A specific voxel is encircled by a tiny rectangular window in the pattern matcher that serves as the container.

The algorithm seeks the pattern and template with the lowest distance between them. Its lesser precision is its primary drawback. By [18], 3DVIEWNIX was created. It is a fantastic piece of software for multi-dimensional medical image processing, viewing, modification, and analysis. Filtering, interpolation, segmentation, registration, intensity standardisation, and assessment are just a few of the many jobs it may accomplish. Model-based solutions for segmentation, such as active shape and appearance models, are the main foundation. To concurrently see and qualitatively assess the size and positions of post-surgery brain tissues, a 3DVIEWNIX package dubbed 3DVIEWNIX-TV is capable of displaying two gray-level slices as transparent colour overlays. By using the fuzzy-linked approach, the software may be used in a clinical system for tumour volume assessment [19].

By integrating K-means Clustering for grouping tissues with the Perona-Malik anisotropic diffusion model for image enhancement, Marroquin et al. (2002) created segmentation of brain MRI images for tumour extraction. A fuzzy clustering technique was developed by [21] for the segmentation of brain MRI images. They visually displayed the outcome of their suggested approach, but they did not numerically demonstrate that their results were superior, nor did they evaluate their outcomes in comparison to those of other procedures. Similar to this, a technique for segmenting white matter, grey matter, and CSF areas in MRI images that was proposed by [22] and modified Mumford Shah's segmentation algorithm is used. The standard Mumford Shah's energy function is enhanced by this way using the tuning weight notion. For segmentation into three tissue classes, these weights need to be adjusted. Brain MRI segmentation into three tissues is done one tissue at a time rather than all three at once. For Mumford Shah's energy function parameter initialization, this technique also requires training from manually segmented pictures. Only T1 weighted photos may be used with this technique. Due to the poor contrast of T1 weighted images, manual seeding is necessary for initialization. This approach cannot be used for all types of brain MRI images, such as T2 weighted and PD pictures, due to manual seeding and training using manually segmented data. To enhance lung tumour segmentation with PET, [23] created a segmentation energy function for the graph cuts approach. A standardised uptake value (SUV) cost function, a monotonic downhill SUV feature, and an examination of the tumour voxels in PET scans served as the foundation for their segmentation strategy. The SUV cost function enhances the border definition and also takes into account cases when the lung tumour is heterogeneous. The monotonic downhill feature prevents segmentation leakage into neighbouring tissues with equal or greater PET tracer uptake than the tumour. 42 clinical PET volumes from non-small cell lung cancer patients were used to assess the technique (NSCLC). Their strategy outperforms region-growing techniques, the watershed technique, fuzzy-c-means, region-based active contour, and tumour tailored downhill in terms of segmentation. An automated technique for the segmentation of oncological PET data has also been reported by [24]. The Bayesian information criterion (BIC) was first used to choose the best segmentation level. The next step was performing expectation maximisation (EM)-based mixture modelling using the k-means clustering method, which alters the original voxel order. This segmentation was subsequently improved using a multiscale

Markov model by simulating the spatial correlations between adjacent picture voxels. In order to achieve high performance, a co-processing-based field programmable gate array (FPGA) solution was also suggested. It offloads the most complicated calculations hardware. In their study, a hardware-assisted co-processing spatial segmentation system was developed. Using a combination of image wavelet scales and a Markov random field model (MRFM), this system, designed for PET volume analysis, was able to segment data depending on how adjacent voxels are related to one another. To analyse visual structures that could not be seen by modelling in the spatial domain, wavelet approach was used. FPGAs were used to provide the hardware acceleration, and a suitable host application was used to combine the hardware-software co-design process. [25] created a segmentation-by-registration approach whereby a scan of normal lungs was elastically registered to a scan that included pathology. The problematic lungs were separated when the next restoration was carried out on a mask of the normal lungs. A probabilistic segregation created from the segmentations of 15 recorded standard images was used as a mask for the typical lungs. Voxel classification was carried out on a specific volume around the boundaries of the modified probabilistic mask in an effort to improve the segregation. The way in which this approach was put into practise was compared to the ways in which three parallel techniques—conservative, user-interactive, and voxel categorization—were put into practise. Ten three-dimensional thin-slice computed CT volumes with superior-density pathologies were used to test the methods. By comparing the resulting segregations to the physical segmentations in terms of volumetric overlap and border location parameters, the segregations were evaluated. Voxel categorization and the updated segmentation-by-registration outperformed the conservative and user-interactive procedures that began with thresholding methods in their ability to separate the disorders. [26] proposed an automated method using computational geometry methods to distinguish between cracks shown on CT scans. With the aim of improving the pulmonary fissures by reducing non-fissure configurations while smoothing the surfaces of lung fissures, Laplacian smoothing was applied iteratively after a geometric modelling of the lung volume using the marching cubes approach. After that, a comprehensive Gaussian image-based process was used to identify the fissures in a statistical method that approximated the fissures using a collection of plane "patches." The novel technique had many advantages, including the independence of anatomic knowledge of the lung structure aside from the surface shape of fissures, limited sensitivity to parallel lung configurations, and ease of implementation. With the use of a collection of 100 pictures (slices) randomly selected from 10 screening CT scans, the effectiveness of the procedure was evaluated by two expert thoracic radiologists. [27] described a two-step approach for lobe segmentation that used wavelet transform to identify the fissure locales and curvatures inside the relative zones and adaptive fissure sweeping to find fissure zones. The unique approach brought about an accuracy of 76.7%-94.8% with strict evaluation criteria when tested on isotropic CT image stacks from nine unnamed individuals with diseased lungs. On the other hand, surgeons were able to locate the fissure zones with an accuracy of 80% in clinical CT scans with a thickness of 2.5–7.0 mm. Additionally, this article describes how to use the segmentation approach and the programme Amira to see lung lobes in three dimensions. Each patient needed to go through the procedure, including the segregation, in around 5 minutes. The intriguing results offered hope for developing an automated method to separate lung lobes for surgical planning to treat lung cancer. Several broad inferences about system components that may be employed to enhance lung detection performance can be made based on the body of available work. To effectively find tumours, tumour segmentation must move toward a completely automated process. Although the stated accuracy of the suggested automated techniques (in the literature study) for segmenting lung tumours is highly encouraging, these methods still have not been widely adopted by pathologists for regular clinical practise. The lack of standardised processes and the inability of the current approaches to support medical decisions in a clear and understandable manner may be the causes. These difficulties from the literature review are taken into consideration in the current work, which focuses on tumour

identification via image enhancement, tumour segmentation, and tumour classification.

3. Anatomy of the Lungs

The lungs are an organ in the chest that resembles a sponge and functions well as a component of the respiratory system. In order to provide room for the heart, the left lung has two lobes whereas the right lung has three lobes. Air enters the body via the nose or mouth, travels through the trachea and each bronchus, and then enters the lungs. The lungs are two cone-shaped, sponge-like organs. When air is breathed, oxygen is taken up into the lungs. The blood then transports oxygen to the other bodily organs through lung tissue. Carbon dioxide is released by cells when they take up oxygen. Carbon dioxide is carried back to the lungs by the circulation and then leaves the body when air is breathed. In Figure.4, the lung's anatomy is shown.

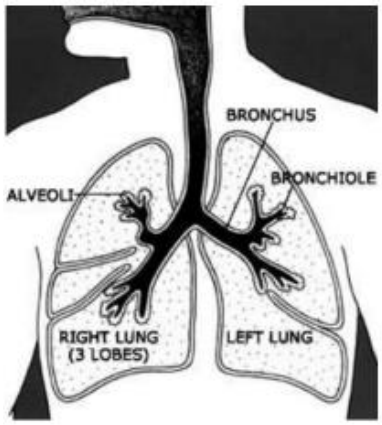

Figure.4. Anatomy of lung

On CT scans, the lung, the location of gas exchange, is filled with air that seems to have a low density (approximately 1000 HU). In addition to air, the main components of the lung regions include pulmonary arteries and bronchi. The left and right lungs are included in the lung regions. An oblique fissure further divides the left lung into its two lung lobes (upper lobe and lower lobe). Oblique and horizontal fissures divide the right lung into three lung lobes (upper lobe, middle lobe, and lower lobe). In the human chest, the bronchial airways' architecture may be roughly compared to a binary tree structure. The left and right principal bronchi, which enter the right and left lungs, are divided into two by the trachea, the airway tree's base. The five (two left, three right) lobar bronchi that enter each lobe of the lung are further divided into the main bronchi. In each lung area, the lobar bronchi repeatedly split, creating 8–10 segmental bronchi trees. Similar to the bronchial airway, the pulmonary arteries and veins are likewise dispersed throughout the lung regions in a tree-like pattern. The branch of the pulmonary artery always runs parallel to the bronchi.

4. Lung Tumour Types

These days, lung cancer is one of the leading causes of rising child and adult mortality. Figure.5. displays the tumour incidence across different age groups. Additionally, lung cancer is a condition in which aberrant cells multiplie rapidly and form tumours. Blood or lymph fluid, which envelops the lung tissue, may carry cancer cells out from the lungs. When a cancer cell leaves the initial location of its growth and moves into a lymph node or to another area of the body through the circulation, this is known as metastasis. Figure.6. shows the historical 5-year survival rates.

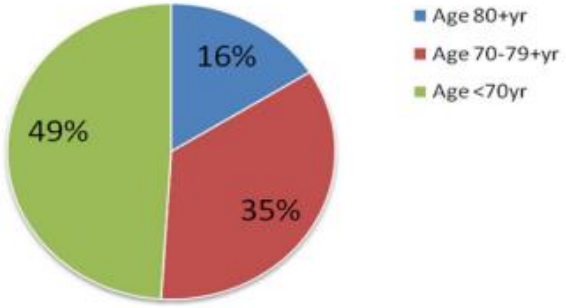

Figure.4. Age distribution of lung cancer

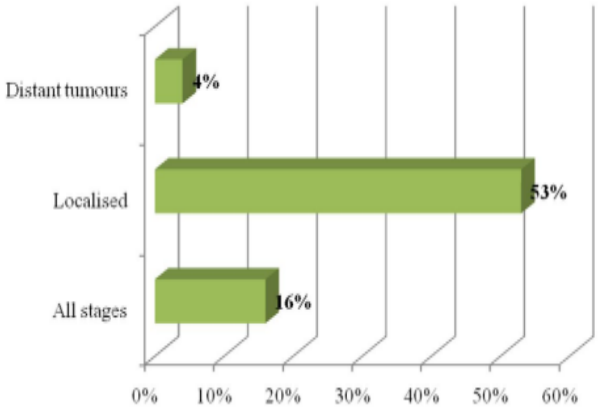

Figure.6. Lung cancer 5-Year survival rates

Lung cancer that starts there is referred to as primary lung cancer. Although there are many other classifications of the illness, they may be divided into two major groups, as seen below: A benign tumour is a collection of cells that cannot infiltrate or spread to nearby tissue. Because a tumour must exhibit these traits in order to be classified as malignant, benign tumours are not cancerous. Additionally, benign tumours often develop more slowly than malignant tumours and typically contain more differentiated tumour cells (cells have normal features). Most benign tumours either stay with the epithelium or have an outside surface (a fibrous sheath of connective tissue) around them. Even while benign tumours may not spread locally or infiltrate nearby tissues, certain varieties can nonetheless have a severe impact on health. A "mass effect" caused by benign tumour development may compress tissues, harming nerves, reducing blood flow to a region of the body, and even resulting in tissue death and organ damage. If a tumour is located in an enclosed area like the skull, respiratory system, sinus, or within bones, its bulk impact will be more noticeable. Although the majority of benign tumours are not life-threatening, several different benign tumour forms have the capacity to develop (or become malignant) over time. Cancer is most often described as having malignancy. A malignant tumour has uncontrolled development, the ability to invade nearby tissues, and the potential to spread to distant regions. Invasiveness and metastasis are characteristics of cancer that is malignant. Genome instability is another characteristic of malignant tumours. Figure.7. displays the CT lung scan with the tumour.

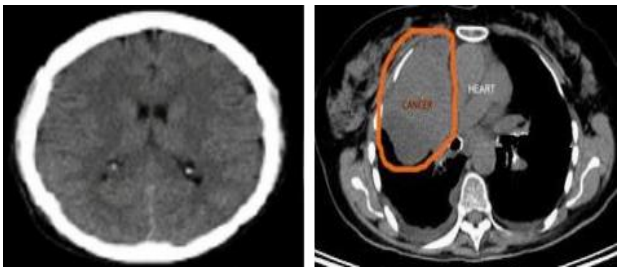

Figure.7. CT scan images (a) normal patient (b) tumour patient, Lung fields (right and left) and tumour area marked by red lines

The potential for invasion plays a key role in determining whether a tumour is benign or malignant. A tumour is benign if it cannot move to distant places by metastasis or invade nearby tissues, while invasive or metastatic tumours are malignant. Because of this, benign tumours are not considered cancer. Benign tumours will develop in a confined space, often enclosed in a capsule of fibrous connective tissue. Both benign and malignant tumours have different growth rates; benign tumours often develop more slowly than malignant tumours. Malignant tumours are more dangerous to your health than benign tumours, although both may be fatal under specific circumstances. Both benign and malignant tumours have a number of common traits, however sometimes one form may exhibit traits of the other. For instance, dangerous tumours are often undifferentiated whereas benign tumours are typically highly differentiated. However, it is possible to have both differentiated malignant tumours and undifferentiated benign tumours. Despite the fact that benign tumours typically develop slowly, fast-growing benign tumours have nevertheless been reported in certain situations. Some cancerous tumours, including basal cell carcinoma, are often non-metastatic.

5. Tumour Segmentation Algorithm

Cellular automata (CA) with a level set evaluation-based seeded segmentation approach is used to extract the lung tumour area. The fascinating characteristics of cellular automata Smith (1976), such as their local nature and straightforward parallel computation implementation, make them seem to be suitable instruments for image processing [29]. Numerous articles on the subject of cellular automata for image processing are available. In this application for lung tumour identification, CA and level set are merged and utilised to extract the tumour area. The tumour area segmentation is carried out using the following sets of stages. Figure.8 shows the suggested algorithm's total segmentation.

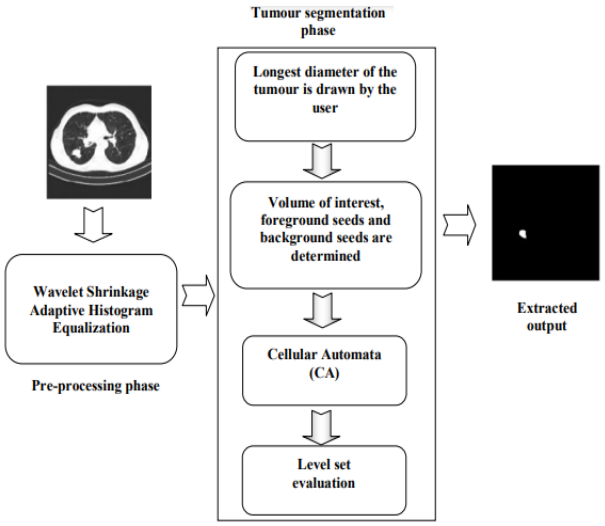

Figure.8. Block diagram of proposed segmentation algorithm

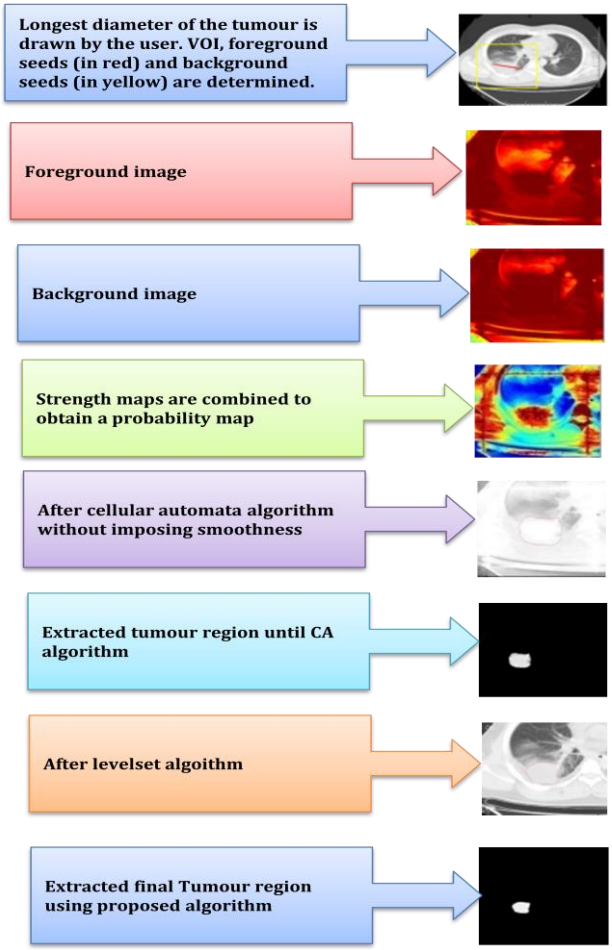

Figure.9. Steps involved in the proposed segmentation process

The ensuing Figure 9 lists the intermediate stages and accompanying outcomes. A level set surface is initially initialised at 0.5 HT and the map HT is used to evolve the surface which converges to the final segmentation. (a) First, the input image is taken. (b) A tumour CA algorithm is run on the VOI for each two sets of seeds (for the foreground and background). This results in strength maps for the foreground (c) and background (d).

Choosing the seed locations to launch the tumour area extraction procedure is a crucial step in the proposed tumour segmentation method. The longest in-plane tumour diameter in one dimension is used to classify tumour progress in "Response Evaluation Criteria in Solid Tumours," a commonly used method to assess the treatment response of solid tumours (axial, coronal, sagittal). The pixel values are used to calculate the background and tumour seeds [30]. The volume of interest (VOI), the tumour seeds, and the background seeds are determined by using the line already drawn by the user to measure the longest diameter of the solid tumour. The proposed seed selection algorithm uses the same concept to follow the familiar clinical routine to which the clinicians are accustomed. Similar to this, the seed selection process for the tumour segmentation challenge begins with a single line that the user draws along the tumor's largest visible diameter. The VOI and seeds are then calculated as follows: I The line is cropped by 15% from each end and thickened to three pixels wide to obtain tumour seeds; ii) The VOI is chosen as the bounding box of the sphere having a diameter 35% longer than the line; and iii) a one-voxel-wide border of this VOI is used as background seeds.

6. Tumour Classifier

In this paper , a comprehensive intelligent classification method dubbed the CALMKSVM tumour classifier is suggested and used to lung images. Pre-processing, tumour segmentation, feature extraction, and classification are the four key stages that make up the CAL-MKSVM tumour classifier's suggested methodology. In order to prepare the input CT lung picture for further image processing processes, Wavelet Shrinkage Adaptive histogram Equalization (WSAHE) is initially used. The lung tumour is then isolated using a seeded segmentation technique based on cellular automata (CA). The

segmented benign and malignant tumour lung pictures are used to construct the wavelet-based second-order statistics characteristics. The multi-kernel support vector machine (MKSVM) is then utilised to determine the benign or malignant nature of the input CT tumour picture. The experimental findings demonstrate that the CAL-MKSVM tumour classification approach has surpassed current strategies by being more accurate.

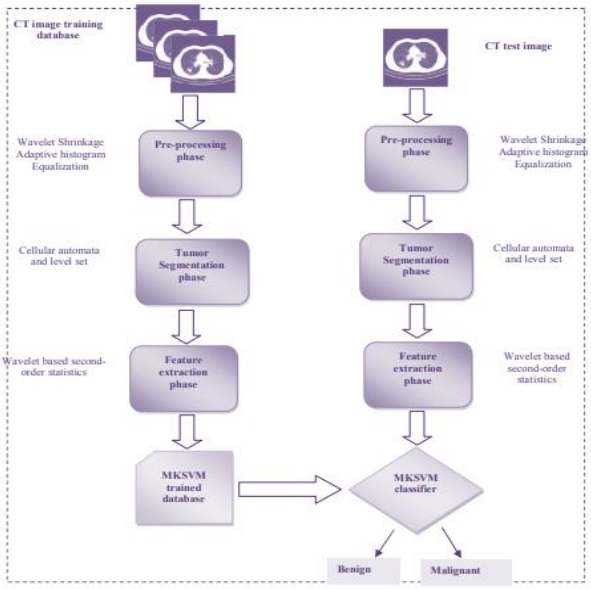

Figure.10. Illustration of the proposed CAL-MKSVM tumour classifier

For both men and women, lung cancer is the leading cause of cancer-related mortality. The best chance for a patient to survive beyond lung cancer is early identification. Recent years have seen the development of a wide range of literature on tumour detection methods. The CAL-MKSVM tumour classification method, which makes use of cellular automata and support vector machines, is proposed in this section. Four steps make up the CAL-MKSVM technique as it is now being put forth: I pre-processing; (ii) tumour segmentation; (iii) feature extraction; and (iv) classification. Figure.10 shows the block diagram of the suggested strategy.

7. Results and Discussion

This section presents the experimental findings of the suggested lung tumour segmentation method employing hybridization of CA with level set. The suggested method uses Matlab programming for tumour identification (Matlab Version 2021). The experimental findings are shown using a variety of medical photos gathered from hospitals. Images from a computed tomography (CT) scan of the lung are used in the tumour identification method. The segmented output for several sizes of medical pictures, including 512 x 512 and 128 x 128 has higher segmentation accuracy (SA), spatial overlap, and jaccard coefficient. The obtained findings demonstrated the viability of the suggested strategy. The segmentation methods that are currently in use are used to conduct the robustness and comparative analyses.

For this study, the computed tomography (CT) data set was gathered in the South Indian region at S.P.Scans Advanced CT & MRI and Pranav Scans. Patients with benign and malignant tumours have different CT pictures taken of them. This image data collection contains 100 CT pictures of lung tumours, including 63 images of malignant tumours and 37 photos of benign tumours. The data set for CT lung images is split into two sets: (1) training data and (2) testing data. The lung tumour pictures are segmented using the training data set, and the presentation of the suggested method is examined using the testing data set. In this instance, several training and testing ratios are tried for validity.

7.1 Evaluation Metrics

The suggested method carries out the numerical outcomes in terms of performance indicators such as the Jaccard coefficient, spatial overlap, and segmentation accuracy, which are computed for each segment of the tumour. The segmented tumor's output is compared to the actual data (target). The user manually ascertains the ground truth. Equations (1), (2), and (3) are used to analyse the severity of 16 CT lung tumour pictures using performance metrics such the Jaccard coefficient, spatial overlap, and segmentation accuracy (3).

$$\text{Spatial overlap SO} = \frac{2\,(A \cap B)}{A + B} \ldots\ldots (1)$$

$$\text{Jaccard coefficient J}\,(X, Y) = \frac{|(A \cap B)|}{(A \cup B)} \ldots\ldots (2)$$

$$\text{Segmentation Accuracy (SA)} = \frac{(\text{No. of pixels matched})}{(\text{Total no. of Tumour pixels in ground truth})} \text{ x } 100 \ldots\ldots (3)$$

where, A is the pixels of proposed approach tumour image B is the pixels of manual

segmented image. The direct ratio of the output of the suggested approach to the total number of tumour pixels in the ground truth is used to calculate the segmentation accuracy. Figure.11. demonstrates the segmentation outcomes for 16 CT images using the suggested and current methods.

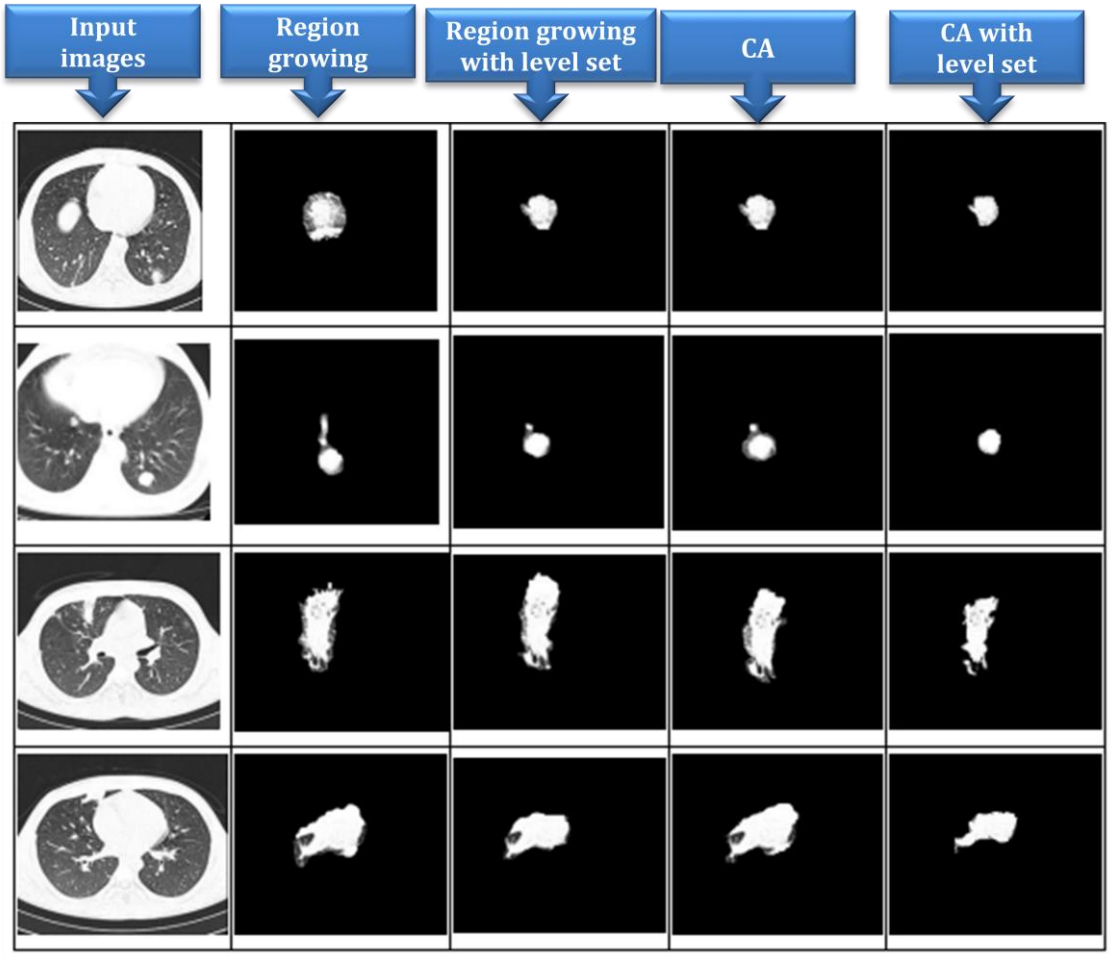

Figure.11. Segmentation results of the proposed against the existing systems

Comparative analysis is done between the suggested system, cellular automata with level set, and three other systems, including region growing, cellular automata, and hybridization of region growing with level set. Table.1. displays a comparison of the proposed and current systems' segmentation accuracy. Table.2. compares the suggested systems' Jaccard Coefficient findings to those of the current ones. Table.3. shows the results of the geographic overlap between the planned and current systems.

Table.1. Segmentation accuracy comparison of the proposed against the existing systems

Segmentation accuracy (%)				
Input images	Region growing	Region growing with level set	CA	CA with level set
	80.25	85.24	85.65	90.12
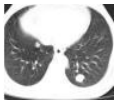	80.34	84.65	85.12	90.13
	80.47	85	85.14	90.014
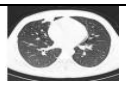	81.24	84.63	82.35	90.45

Table.2. Jaccard Coefficient comparison of the proposed against the existing systems

Jaccard Coefficient				
Input images	Region growing	Region growing with level set	CA	CA with level set
	0.67	0.71	0.81	0.821
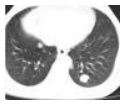	0.58	0.72	0.79	0.824
	0.68	0.74	0.76	0.842
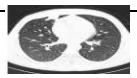	0.78	0.72	0.73	0.842

Table.3. Spatial overlap comparison of the proposed against the existing systems

Spatial Overlap (SO)				
Input images	Region growing	Region growing with level set	CA	CA with level set
	0.682	0.61	0.64	0.84
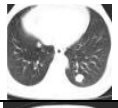	0.56	0.64	0.68	0.897
	0.76	0.62	0.68	0.82
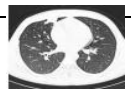	0.71	0.63	0.69	0.85

8. Conclusion

One of the trickiest issues in medical picture analysis is object segmentation. This paper demonstrates an entirely intelligent method for tumour identification using the automated lung tumour segmentation technique. On computed tomography (CT) images, a cellular automata (CA)-based seeded tumour segmentation approach and seed selection was developed, which standardises the volume of interest (VOI). To enhance the shortest route issue, links between cellular automata-based segmentation and graph-theoretical techniques are initially developed. In light of this, the cellular automaton's state transition function is modified to determine the best shortest route. With the help of a data collection of aberrant CT scans, the suggested technique is put to the test, and the outcomes are contrasted with those of alternative approaches based on artificial neural networks and K-nearest neighbour classifiers. Additionally, an implicit level set surface was produced on a cancer probability map created from CA states to enforce spatial smoothness, and a sensitivity parameter is started to adjust to the heterogeneous tumour segmentation challenge. The final tumour area was recovered from the computed tomography images based on the level set surface. The experimental finding demonstrates that the suggested technique outperforms the segmentation algorithms that are already in use.

References

1. Alan Wee-Chung Liew & Hong Yan 2006, 'Current Methods in the Automatic Tissue Segmentation of 3D Magnetic Resonance Brain Images' Current Medical Imaging Reviews, vol.2, pp.1-13.
2. Ahmed, M M & Mohamad, D B 2008, 'Segmentation of Brain MR Images for Tumour Extraction by Combining Kmeans Clustering and Perona-Malik Anisotropic Diffusion Model,' International Journal of Image Processing, vol.2, no.1, pp.27–34.
3. Anbeek, P, Vincken, K L, van Osch, M J P, Bisschops, R H C & van der Grond, J 2004, 'Automatic segmentation of different-sized white matter lesions by voxel probability estimation,' Med. Image Anal., vol.8, pp. 205–215.
4. Bach, F 2008, 'Exploring Large Feature Spaces with Hierarchical Multiple Kernel Learning,' Advances in Neural Information Processing Systems (NIPS), pp.105–112.
5. Bellon, E, Feron, M, Maes, F, Hoe, LV, Delaere, D, Haven, F, Sunaert, S, Baert, A, Marchal, G & Suetens, P 1997, 'Evaluation of manual vs. semi-automated delineation of liver lesions on CT images', European Radiology, vol.7, pp.432–438.

6. Beare, R, Srikanth, V, Chen, J, Phan, T G, Stapleton, J, Lipshut, R & Reutens, D 2009, 'Development and validation of morphological segmentation of age-related cerebral white matter hyperintensities', NeuroImage, vol. 47, pp. 199–203.
7. Charnoz, A, Agnus, V, Malandain, C, Forest, M, Tajine, L & Soler 2005, 'Liver registration for the follow-up of hepatic tumours', Medical Image Computing and Computer-Assisted Intervention, vol. 3750, pp.155–162.
8. Chunming Li, Rui Huang, Zhaohua Ding, J, Chris Gatenby, Dimitris, N & John C Gore 2011, 'A Level Set Method for Image Segmentation in the Presence of Intensity Inhomogeneities With Application to MRI', IEEE Transactions On Image Processing, vol. 20, no. 7.
9. Cobzas D, Birkbeck N, Schmidt M, Jagersand, M & Murtha, A 2007, '3-D variational brain tumour segmentation using a high dimensional feature set', in Proc. IEEE 11th Int. Conf. Comput. Vision, pp. 1–8.
10. Dubey, RB, Hanmandlu, M & Gupta, SK 2009, 'Semi-automatic Segmentation of MRI Brain Tumour', ICGST-GVIP Journal, vol.9, no.4, pp.33–40.
11. De Boer, R, Vrooman, HA, van der Lijn, F, Vernooij, MW, Ikram, MA, van der Lugt, A, Breteler, MMB & Niessen, WJ 2009, 'White matter lesion extension to automatic brain tissue segmentation on MRI', NeuroImage, vol. 45, pp. 1151–1161.
12. Deniz Aykac, Eric, A, Hoffman, Geoffrey McLennan & Joseph M Reinhardt 2003, 'Segmentation and Analysis of the Human Airway Tree from Three-Dimensional X-Ray CT Images', IEEE Transactions On Medical Imaging, vol. 22, no. 8.
13. Foruzan, A H, Zoroof, R A, Hori, M & Sato, Y 2009, 'A knowledge-based technique for liver segmentation in CT data', Comp. Med. Imaging Graph., vol.33, no.8, pp.567–587.
14. Gerig, G, Kubler, O, Kikinis, R & Jolesz, FA 1992, 'Nonlinear anisotropic filtering of MRI data', IEEE Transactions on Medical Imaging, vol.11, pp.221–232.
15. Gloger, O, Kühn, J, Stanski, A, Völzke, H & Puls, R 2010, 'A fully automatic three-step liver segmentation method on LDA-based probability maps for multiple contrast MR images', Magn. Reson. Imaging, vol.28, no.16, pp.882–897.
16. Hamamci, A & Unal, G 2012, 'Multimodal brain tumour segmentation using the tumour-cut method on the BraTS dataset', in Proc. MICCAIBRATS, pp. 19–23.
17. Jiantao Pu, Joseph, K, Leader, Bin Zheng, Friedrich Knollmann, Carl Fuhrman, Frank, C, Sciurba & David Gur 2009, 'A Computational Geometry Approach to Automated Pulmonary Fissure Segmentation in CT Examinations', IEEE Transactions On Medical Imaging, vol. 28, no. 5.
18. Keita Nakagomi, Akinobu Shimizu, Hidefumi Kobatake, Masahiro Yakami, Koji Fujimoto & Kaori Togashi 2013, 'Multi-shape graph cuts with neighbor prior constraints and its application to lung segmentation from a chest CT volume', Medical Image Analysis, vol.17, pp.62–77.
19. Kaus, MR, Warfield, SK, Nabav, A, Black, PM, Jolesz, FA & Kikinis, R 2001, 'Automated segmentation of MR images of brain tumours', Radiology, vol. 218, no. 2, pp. 586–591.
20. Lu, R, Marziliano, P & Thng, CH 2005, 'Liver tumour volume estimation by semiautomatic segmentation method', In: Proceedings of the 2005 IEEE Engineering in Medicine and Biology 27th Annual Conference, pp. 3296–3299.
21. Luo, S, Hu, Q, He, X, Li, J, Jin, JS & Park, M 2009, 'Automatic liver parenchyma segmentation from abdominal CT images using support vector machines', in: Proceedings of International Conference on Complex Medical Engineering (ICME), Tempe, AZ, USA, pp. 1–5.
22. Mohsen Keshani, Zohreh Azimifar, Farshad Tajeripour & Reza Boostani 2013, 'Lung nodule segmentation and recognition using SVM classifier and active contour modeling: A complete intelligent system', Computers in Biology and Medicine, vol.43, pp.287–300.
23. Prasad, S & Jhaveri, K2002, 'CT tumour measurement for therapeutic response assessment: comparison of unidimensional, bidimensional, and volumetric techniques initial observations', Radiology, vol.225, vol.2, pp.416–419.

24. Rafael Molina, Miguel Vega, Javier Mateos & Aggelos K Katsaggelos 2006, 'Parameter Estimation in Bayesian Reconstruction of Multispectral Images Using Super Resolution Techniques', In proceedings of IEEE International Conference on Image Processing, pp.1749-1752.
25. Ratan, R, Sharma, S & Sharamac, Sk 2009, 'Brain tumour detection based on multi-parameter MRI image analysis', ICGST-GVIP Journal 9(III), pp. 9–17.
26. Rina, D, Rudyanto, Gorka Bastarrika, Gabriel de Biurrun, Jackeline Agorreta, Luis, M, Montuenga, Carlos Ortiz-de-Solorzano & Arrate Muñoz-Barrutia 2013, 'Individual nodule tracking in micro-CT images of a longitudinal lung cancer mouse model', Medical Image Analysis, vol.17, pp.1095–1105.
27. Sema Candemir, Stefan Jaeger, Kannappan Palaniappan, Jonathan, P, Musco, Rahul, K, Singh, Zhiyun Xue, Alexandros Karargyris, Sameer Antani, George Thoma & Clement J McDonald 2014, 'Lung Segmentation in Chest Radiographs Using Anatomical Atlases With Nonrigid Registration', IEEE Transactions On Medical Imaging, vol. 33, no. 2.
28. Shanhui Sun, Milan Sonka, Reinhard, R & Beichel 2013, 'Lung segmentation refinement based on optimal surface finding utilizing a hybrid desktop/virtual reality user interface', Computerized Medical Imaging and Graphics, vol.37, pp.15– 27.
29. Tran, LN, Brown, M.S, Goldin, JG, Yan, X, Pais, RC, McNitt-Gray, MF, Gjertson, D, Rogers, SR & Aberle, DR 2004, 'Comparison of treatment response classifications between unidimensional, bidimensional, and volumetric measurements of metastatic lung lesions on chest computed tomography', Academic Radiology, vol.11, no.12, pp.1355–1360.
30. Therasse, P, Arbuck, SG, Eisenhauer, EA, Wanders, J Kaplan, RS, Rubinstein, L, Verweij, J, Van Glabbeke, M, van Oosterom, AT, Christian, MC & Gwyther, SG 2000, 'New guidelines to evaluate the response to treatment in solid tumours', Journal of the National Cancer Institute, vol.92, no.3, pp.205–216.